Metallophysics and Advanced Technologies
Металофіз. новітні технол.
Metallofiz. Noveishie Tekhnol.
2023, vol. 45, No. 9, pp. 1067–1082
https://doi.org/10.15407/mfint.45.09.1067
Reprints available directly from the publisher

PACS numbers: 71.15.Mb, 71.20.Ps, 75.50.Ee, 78.20.Fm, 78.20.Ls, 78.70.Dm, 81.05.Zx

Electronic Structure and X-Ray Magnetic Circular Dichroism in *A*-Site Ordered Perovskite $CaCo_3V_4O_{12}$

D. V. Mazur*, L. V. Bekenov*, B. Kh. Zhuravlov*, S. V. Mokliak*, Yu. M. Kucherenko*, and V. M. Antonov*,**

**G. V. Kurdyumov Institute for Metal Physics, NAS of Ukraine,*
36 Academician Vernadsky Blvd.,
UA-03142 Kyiv, Ukraine
***Max-Planck-Institut für Festkörperforschung,*
1 Heisenbergstr.,
D-70569 Stuttgart, Germany

We are studied the electronic and magnetic properties of the *A*-site ordered perovskite $CaCo_3V_4O_{12}$ within the density-functional theory using the generalized gradient approximation (GGA) with the consideration of strong Coulomb correlations (GGA + *U*) in the framework of the fully relativistic spin-polarized Dirac linear muffin-tin orbital method of band-structure calculation. The x-ray absorption spectra and x-ray magnetic circular dichroism at the Ca, Co, and V *K*-edges are investigated theoretically. The effect of the electric quadrupole E_2 transitions and magnetic dipole M_1 transitions are analysed. The calculated results are in good agreement with experimental data.

Key words: electronic band structure, magnetic moment, GGA, x-ray absorption spectra, x-ray magnetic circular dichroism, double perovskites.

Електронні та магнетні властивості впорядкованого за *A*-позицією перовськіту $CaCo_3V_4O_{12}$ досліджено в рамках теорії функціоналу густини з використанням узагальненого ґрадієнтного наближення з урахуванням сильних Кулонових кореляцій (GGA + *U*) у рамках повністю релятивістського спін-поляризованого Діракового ЛМТО-методу розрахунку зонної структури. Теоретично досліджено Рентґенові спектри поглинання та Рентґенів магнетний циркулярний дихроїзм на Ca-, Co- та V-*K*-краях.

Corresponding author: Dmytro Viktorovych Mazur
E-mail: mazur.dm.v@gmail.com

Citation: D. V. Mazur, L. V. Bekenov, B. Kh. Zhuravlov, S. V. Mokliak, Yu. M. Kucherenko, and V. M. Antonov, Electronic Structure and X-Ray Magnetic Circular Dichroism in *A*-Site Ordered Perovskite $CaCo_3V_4O_{12}$, *Metallofiz. Noveishie Tekhnol.*, **45**, No. 9: 1067–1082 (2023). DOI: 10.15407/mfint.45.09.1067

Проаналізовано вплив електричних квадрупольних E_2-переходів і магнетних дипольних M_1-переходів. Результати розрахунків добре узгоджуються з експериментальними даними.

Ключові слова: електронна зонна структура, магнетний момент, узагальнена ґрадієнтна апроксимація, спектри поглинання Рентґенових променів, Рентґенів магнетний циркулярний дихроїзм, подвійні перовськіти.

(Received 1 September, 2023; in final version, 22 September, 2023)

1. INTRODUCTION

Transition-metal perovskites have been studied for half a century, and most intensively during the last decade, for their fascinating electronic and magnetic properties arising from narrow 3*d* bands and strong Coulomb correlations [1–5]. Perovskite-structure oxides with the general formula ABO_3 display a large variety of intriguing properties and raise lots of important fundamental issues in solid-state physics and chemistry. The structure can be described as a framework of corner-sharing BO_6 octahedra that has an *A*-site cavity formed by twelve coordinated oxygen ions. The smaller *B*-site cations have octahedral coordination by the O anions. The octahedra share corners to form a three-dimensional network, while the larger *A*-site cations sit in the 12-co-ordinate cubooctahedral cavities within this network. Perovskites display a wide range of properties including superconductivity (*e.g.*, $Ba_{1-x}K_xBiO_3$), colossal magnetoresistance (*e.g.*, $La_{1-x}Ca_xMnO_3$), itinerant electron ferromagnetism (*e.g.*, $SrRuO_3$), multiferroic behaviour (*e.g.*, $TbMnO_3$), ferroelectricity (*e.g.*, $BaTiO_3$), piezoelectricity (*e.g.*, $PbZr_{1-x}Ti_xO_3$), and ionic conductivity (*e.g.*, $La_{0.67-x}Li_{3-x}TiO_3$, $BaCeO_{3-x}$). Perovskites arguably represent the most important family of complex oxides. Distortions from the ideal perovskite structure can significantly influence the physical properties. Octahedral tilting distortions, which are present in 80–90% of all perovskites, occur when the *A*-site cation is too small for the cubooctahedral cavities [6, 7]. The octahedral tilting distortions alter the conduction bandwidth [8] and the strength of the magnetic super-exchange interactions [9]. As such, they provide a mechanism for fine-tuning the electrical, magnetic and optical properties.

More sophisticated double perovskites, *e.g.*, those that are called '*A*-site ordered' with the general formula $A(A')_3B_4O_{12}$, comprise one more site (*A*′) for cations with unusual two-dimensional square oxygen coordination. The *A*-site ordered perovskite-structure oxides $A(A')_3B_4O_{12}$ can be obtained by filling 3/4 of the *A*-sites with small transition-metal cations and the other 1/4 with larger alkali, alkaline earth, or rare earth cations. They have a $2a\times2a\times2a$ structure stabilized by heavy tilted BO_6 octahedra and consequently forming $A'O_4$ square-planar units. Cu and Mn are typical transition-metal cations readily accommodated

by the A' site. Compounds with this structure type were synthesized in the 1960s and 1970s [10, 11], and recently lots of fascinating functional properties have been discovered in this class of compounds. Among them are a large dielectric constant in $CaCu_3Ti_4O_{12}$ [12], a large negative thermal-expansion-like volume change due to interstitial charge transfer in $LaCu_3Fe_4O_{12}$ [13], and multiferroism in $CaMn_3Mn_4O_{12}$ [14]. New A-site ordered perovskites with novel properties have been attracted much attention recently [15]. These perovskites not only have the B–B interaction (or B–O–B interaction *via* oxygen ions) largely responsible for the properties of simple perovskites but also have interactions between the transition-metal ions at the A' sites (A'–A' interaction) and between those at the A' and B sites (A'–B interaction).

Among different families of the A-site ordered $A(A')_3B_4O_{12}$ double perovskites, the most studied to date are compounds with $B = Fe$ because of their nontrivial magnetic properties and charge disproportionation reactions, which can lead to spectacular phenomena [13]. Members of other double-perovskite families, for instance, those of V-based perovskites, $A(A')_3V_4O_{12}$, also find various applications, but they are less systematically studied to date [16, 17]. Recent investigations of some vanadium compounds show that V-based perovskites may reveal rather spectacular and novel physical properties [17, 18].

$CaCo_3V_4O_{12}$ was synthesized by Ovsyannikov *et al.* [19]. It was shown that this new double perovskite possesses high-spin Co^{2+} ions in the $Im\bar{3}$ cubic symmetry. The magnetic susceptibility measured on bulk polycrystalline samples of $CaCo_3V_4O_{12}$ shows a sharp maximum around 98 K, which is a characteristic of an antiferromagnetic (AFM) ordering transition. The authors established that the Co^{2+} ions in $CaCo_3V_4O_{12}$ are in the high-spin state with a sizable orbital moment. Electrical resistivity data suggest semiconducting behaviour in the temperature range of 1.6–370 K. The chemical formula of this perovskite can be written as $Ca^{2+}Co_3^{2+}V_4^{4+}O_{12}^{2-}$. Later Ovsyannikov *et al.* investigated the structural, vibrational, magnetic, and electronic properties of the $CaCo_3V_4O_{12}$ perovskite at low temperatures and high pressure [17]. They found no apparent signatures of metallization of this perovskite up to 60 GPa. From the high-pressure thermoelectric power measurements, its electrical conduction may be described as semi-metallic and strongly compensated. By means of ambient-pressure neutron powder diffraction, the authors established that, below 100 K, $CaCo_3V_4O_{12}$ transforms into an AFM phase, in which all the magnetic moments of the Co^{2+} ions are aligned along the c-axis, and the magnetic structure has a 2-fold periodicity along this axis. They also measured the XAS at the Ca, Co, and V K-edges at 70 and 298 K.

The aim of this paper is the theoretical study from the first principles of the electronic and magnetic structures and x-ray magnetic cir-

cular dichroism in the double perovskite $CaCo_3V_4O_{12}$. The energy band structure of $CaCo_3V_4O_{12}$ is calculated within the *ab initio* approach taking into account strong electron correlations by applying a local spin-density approximation to the density functional theory supplemented by a Hubbard U term (GGA + U) [20].

The paper is organized as follows. The computational details are presented in Sec. 2. Section 3.1 presents the electronic and magnetic structures of $CaCo_3V_4O_{12}$. Section 3.2 presents the theoretically calculated XA and XMCD spectra at the Ca, Co, and V K-edges calculated in the GGA + U approximation. The theoretical results are compared with experimental measurements. Finally, the results are summarized in Sec. 4.

2. CRYSTAL STRUCTURE AND COMPUTATIONAL DETAILS

2.1. X-Ray Magnetic Circular Dichroism

Magnetooptical (MO) effects refer to various changes in the polarization state of light upon interaction with materials possessing a net magnetic moment, including rotation of the plane of linearly polarized light (Faraday or Kerr rotations), and the complementary differential absorption of left and right circularly polarized light (circular dichroism). In the near visible spectral range, these effects result from excitation of electrons in the conduction band. Near x-ray absorption edges, or resonances, the magnetooptical effects can be enhanced by transitions from well-defined atomic core levels to empty valence or conduction states.

Within the one-particle approximation, the absorption coefficient $\mu_{j\lambda}(\omega)$ for incident x-ray polarization λ and photon energy $\hbar\omega$ can be determined as the probability of electronic transitions from initial core states with the total angular momentum j to final unoccupied Bloch states:

$$\mu_{j\lambda}(\omega) = \sum_{mn\mathbf{k}} \left| \left\langle \Psi_{n\mathbf{k}} \left| \hat{\Pi}_\lambda \right| \Psi_{jm} \right\rangle \right|^2 \delta(E_{n\mathbf{k}} - E_{jm} - \hbar\omega)\theta(E_{n\mathbf{k}} - E_F)\,, \qquad (1)$$

where Ψ_{jm} and E_{jm} are the wave function and the energy of a core state with the projection of the total angular momentum m, Ψ_{nk} and E_{nk} are the wave function and the energy of a valence state in the n-th band with the wave vector $\mathbf{k}$, E_F is the Fermi energy. $\hat{\Pi}_\lambda$ is the electron–photon interaction operator in the dipole approximation:

$$\hat{\Pi}_\lambda = -e\boldsymbol{\alpha}\mathbf{a}_\lambda\,; \qquad (2)$$

here, α are the Dirac matrices and $\mathbf{a}_\lambda$ is the λ polarization unit vector of the photon vector potential with $\mathbf{a}_\perp = (1/\sqrt{2}, \pm i/\sqrt{2}, 0)$ $\mathbf{a}_\parallel = (0, 0, 1)$. Here, '+' and '–' denote, respectively, left and right circular photon polarizations with respect to the magnetization direction in the solid.

Then, x-ray magnetic circular and linear dichroism are given by $\mu_+ - \mu_-$ and $\mu_{\|} - (\mu_+ + \mu_-)/2$, respectively. More detailed expressions for the matrix elements within the electric-dipole approximation may be found in Refs. [21–23]. The matrix elements due to magnetic dipole and electric quadrupole corrections are presented in Ref. [23].

2.2. Crystal Structure

The crystal structure of $CaCo_3V_4O_{12}$ shown in Fig. 1 can be considered as a variant of the cubic perovskite oxide ABO_3. The superstructure $A(A')_3B_4O_{12}$, with space group $Im\bar{3}$ (No. 204), is formed by quadrupling the parent unit cell and replacing 3/4 of the element A with A'. Due to the introduction of A', the symmetry of the structure is lowered by a large rotation of the BO_6 octahedra, which brings four oxygen ions closer to the A'(Co) site to form a seemingly nearly square-planar environment. This particular quadruple perovskite house VO_6 octahedra, which are virtually regular: all V–O distances are identical, and the O–V–O angles deviate from 90° by only 0.04° [19]. The CoO_4 plaquettes are not so regular, with the O–Co–O angles being 93.6° and 86.4°. The V ions separated by $a/2$ lie on a simple cubic sublattice, while the Co ions lie on a b.c.c. sublattice with the same nearest-neighbour Co–Co distance. The two perovskite A and B sublattices form a CsCl configuration, making it likely that nearest-neighbour Co–V exchange interactions (*versus* Co–Co or V–V) are the driving force for the magnetic order [24]. The crystal parameters of $CaCo_3V_4O_{12}$, which are used in our

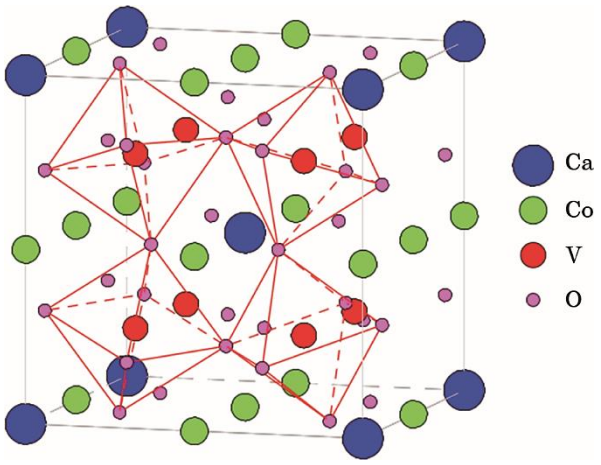

Fig. 1. The crystal structure of $CaCo_3V_4O_{12}$. There is square-planar oxygen coordination of the Co^{2+} ions occupying the A' sites and the octahedral network of V^{4+} ions. The solid lines are the unit cell boundaries.

TABLE 1. Atomic positions of $CaCo_3V_4O_{12}$ at room temperature (lattice constant $a = 7.3428$ Å [19].).

Atom	Site	x	y	z
Ca	2a	0	0	0
Co	6b	0	1/2	1/2
V	8c	1/4	1/4	1/4
O	24g	0	0.2990	0.8115

band structure calculations, are presented in Table 1.

2.3. Calculation Details

The details of the computational method are described in our previous papers [25–28], and here, we only mention several aspects. The band-structure calculations were performed using the fully relativistic linear muffin-tin orbital (LMTO) method [22, 29], which uses four-component basis functions constructed by solving the Dirac equation inside an atomic sphere [30].

The exchange-correlation functional of a GGA-type was used in the version of Perdew, Burke and Ernzerhof (PBE) [31]. The Brillouin zone (BZ) integration was performed using the improved tetrahedron method [32] and the self-consistent charge density was obtained with 1728 **k**-points in the BZ. The basis consisted of Ca, Co, and V s, p, d, and f and O s, p, and d LMTO's.

We found that the agreement between the theoretically calculated and experimentally measured XA and XMCD spectra becomes much better with taking into account strong Coulomb correlations. To include the electron–electron correlations into the consideration we used the 'relativistic' generalization of the rotationally invariant version of the LSDA + U method [33], which takes into account the spin–orbit coupling (SOC) so that the occupation matrix of localized electrons becomes non-diagonal in spin indexes.

This method is described in detail in our previous paper [33] including the procedure to calculate the screened Coulomb U and exchange J integrals, as well as the Slater integrals F^2, F^4, and F^6. In our calculations the intrashell Coulomb repulsion U and interorbital Hund's magnetic coupling J were applied to both Co and V sites: $U_{Co} = 5$ eV, $J_{Co} = 1$ eV, $U_V = 3.4$ eV, $J_V = 0.7$ eV. Similar parameters were used by Rhee and Pickett [24].

The x-ray absorption and dichroism spectra were calculated taking into account the exchange splitting of core levels. The finite lifetime of a core hole was accounted for by folding the spectra with a Lorentzian.

The widths of core levels Γ_K for Ca, Co, and V were taken from [34]. The finite experimental resolution of the spectrometer was accounted for by a Gaussian of 0.6 eV.

3. RESULTS AND DISCUSSION

3.1. Electronic Structure

Since the experimental evidence suggests the AFM order in $CaCo_3V_4O_{12}$ [19], we provide the energy band structure of this double perovskite in the AFM state with and without taking into account the SOC. The results are presented in Fig. 2. The collinear AFM $CaCo_3V_4O_{12}$ ground state within GGA (Fig. 2, *a*, *b*) as well as GGA + SOC (Fig. 2, *c*) is metallic. It is in contradiction to the electrical resistivity data, which suggest semi-conducting behaviour in the temperature range of 1.6–370 K [19].

Adding an on-site Coulomb repulsion on each of the Co and V ions

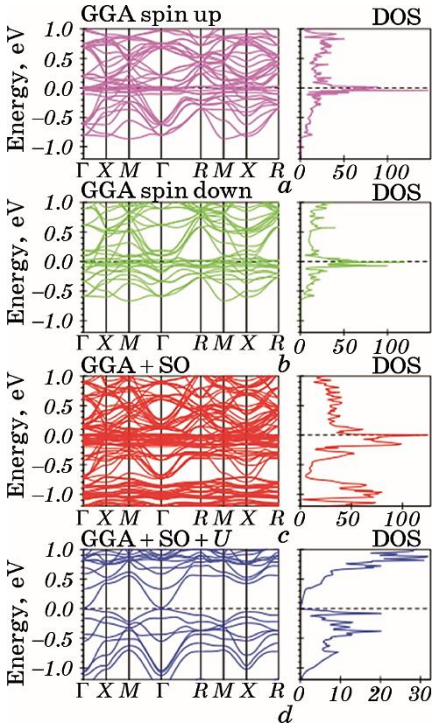

Fig. 2. The energy band structure and total density of states, in states/(cell·eV), of AFM $CaCo_3V_4O_{12}$ calculated in GGA (*a*, *b*), GGA + SOC (*c*), and GGA + SOC + *U* (*d*).

results in a Mott-isolator-type electronic structure of $CaCo_3V_4O_{12}$ (the lower panel of Fig. 2). The energy band gap is rather small and equal to 0.109 eV at the Γ symmetry point.

The crystal field at the Co sites (D_{2h} point symmetry) causes the splitting of Co 3*d* orbitals into five singlets (d_{xz}, d_{xy}, d_{yz}, d_{3z^2-1}, and $d_{x^2-y^2}$). The V site possesses the C_3 point symmetry and V 3*d* states split into one singlet *a* (the combination of d_{xz}, d_{xy}, d_{yz} orbitals) and two doublets d_{3z^2-1}, $d_{x^2-y^2}$ and the combinations of d_{xz}, d_{xy}, d_{yz}.

Both the Co^{2+} and V^{4+} ions in $CaCo_3V_4O_{12}$ are expected to be magnetic and Mott insulating, and carry a substantial orbital moment to account for the observed Curie–Weiss moments. Our calculations reveal that the Mott insulating character of the open-shell Co ions arises mostly through the d_{3z^2-1} orbital with a small amount of $d_{x^2-y^2}$ (see Fig. 3). The partial density of states (PDOS) of V ions is relatively small at the Fermi level.

The Co^{2+} ions are situated in the rectangular CoO_4 plaquettes with the electronic configuration $t_{2g}^5 e_g^2$; therefore, one would expect a large Co orbital moment. From magnetic susceptibility [19] and neutron diffraction measurements of $CaCo_3V_4O_{12}$, the authors of Ref. [17] suggest that the orbital moment at the Co site has to exceed $1\mu_B$. Our band structure calculations confirm this suggestion. We have found that the spin and orbital magnetic moments for the Co_1 ion are $m_s = 2.6062\mu_B$, $m_l = 1.2268\mu_B$, and for the Co_2 ion, they are

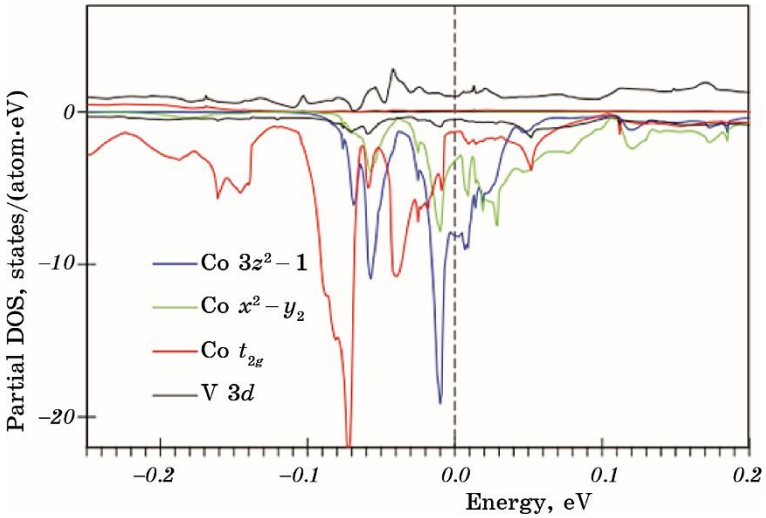

Fig. 3. The symmetry resolved partial density of states, in states/(atom·eV), of AFM $CaCo_3V_4O_{12}$ calculated in GGA.

TABLE 2. The theoretically calculated (in μ_B) spin m_s, orbital m_l, and total m_{total} magnetic moments in $CaCo_3V_4O_{12}$.

Atom	m_s	m_l	m_{total}
Ca_1	0.0086	0.0182	0.0268
Ca_2	0.0040	0.0210	0.0250
Co_1	2.6062	1.2268	3.8330
Co_2	–2.5239	–1.1888	–3.7130
V	1.0360	–0.3082	0.7278
O_1	0.0100	–0.0067	0.0033
O_2	–0.0648	–0.0082	–0.0729

$m_s = -2.5239\mu_B$ and $m_l = -1.1888\mu_B$. The spin and orbital magnetic moments at the V site are equal to $m_s = 1.0360\mu_B$ and $m_l = -0.3082\mu_B$. The Co spin and orbital moments are parallel and the ones at V are antiparallel in $CaCo_3V_4O_{12}$ in accordance with Hund's third rule.

The induced spin magnetic moments at the O_1 and O_2 sites are equal to $0.0100\mu_B$ and $-0.0648\mu_B$, respectively. The orbital magnetic moments are found to be equal to $-0.0067\mu_B$ and $-0.0082\mu_B$ for the O_1 and O_2 sites, respectively. The Ca spin and orbital magnetic moments are rather small for both sites (see Table 2).

Figure 4 presents the partial density of states for $CaCo_3V_4O_{12}$. The O 2*s* states are located mostly between –19.6 eV and –17.8 eV below E_F. The O 2*p* states are situated from –7.9 eV to –1.9 eV, however, a small amount of them appears between –1.9 eV and –1.1 eV as well as from –1.0 eV to 0 eV due to their hybridization with the Co and V 3*d* valence states, respectively. The spin splitting of the oxygen 2*p* states is quite small (around 0.2 eV). The V 3*d* states are situated from –1.2 eV to 0 eV below E_F and from 0.1 eV to 5.4 eV above E_F in the majority spin channel. The spin-down V states are mostly empty and occupy the energy interval from 0.9 eV up to 6.3 eV. There are some V 3*d* occupied states from –7.8 eV to –1.2 eV due to their hybridization with the oxygen 2*p* valence states. The spin-up Co 3*d* states are situated between –7.8 eV and –1.2 eV below E_F. There is a small peak in the close vicinity of E_F in the Co 3*d* states due to their hybridization with V 3*d* states. The Co 3*d* spin-down states occupy the energy interval from –7 eV to –1.5 eV and from 0.8 eV up to 3 eV. The Ca 3*d* empty states occupy the 6.2–8.9 eV energy interval.

3.2. X-Ray Absorption and XMCD Spectra

X-ray absorption and XMCD spectra in metals and alloys at the *K*-

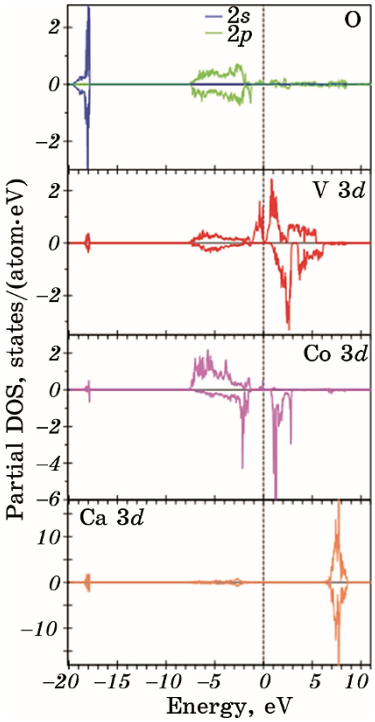

Fig. 4. The partial density of states, in states/(atom·eV), of AFM $CaCo_3V_4O_{12}$ calculated in GGA + SOC + U.

edge, when the 1s core electrons are excited to empty p states through the dipole transitions, are quite important. They are sensitive to the electronic states at neighbouring sites because of the delocalized nature of p states.

Figure 5 presents the partial 4p density of states of Ca, Co, and V ions in $CaCo_3V_4O_{12}$ above E_F calculated in the GGA + SOC + U approximation for the AFM ordering. The 4p DOS in the close vicinity of the Fermi level are quite small. The first peak of 4p DOS starts at 6.8 eV, 10.2 eV, and 12.5 eV for Co, Ca, and V, respectively. The V 4p DOS is the smallest and the one for Ca 4p is the largest. All the PDOSs are extended far above the Fermi level.

The upper panels of Figs. 6, 7 and 8 show the x-ray absorption spectra (open circles) at the Co, V, and Ca K-edges in $CaCo_3V_4O_{12}$ measured at 70 K [17] in comparison with the theoretically calculated ones (full blue lines) in the GGA + SOC + U approximation. The Co K-x-ray-absorption spectrum possesses a major peak at 7726 eV with a low energy shoulder at 7721 eV, two small high-energy shoulders at 7735 eV and 7742 eV, and a high-energy fine structure at 7778 eV (Fig. 6). The theory reproduces the energy position of the major peak and the low

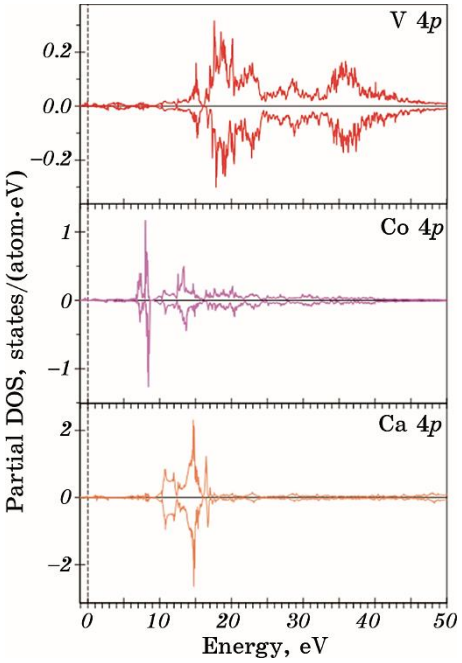

Fig. 5. The partial 4*p* density of states, in states/(atom·eV), of AFM $CaCo_3V_4O_{12}$ calculated in GGA + SOC + *U*.

and high energy shoulders quite well but fails to describe correctly the position of the high energy peak at 7778 eV. The Co *K*-XAS is extended over a very large interval up to 75 eV above the edge, and it is difficult to expect that a linear energy band structure method can describe the spectrum in such a large interval.

The V *K*-x-ray-absorption spectrum possesses two major peaks at 5485 eV and 5502 eV besides a low energy pre-peak at 5470 eV which we discuss later (Fig. 7). The theory reproduces well the energy position of two major peaks. Like in the case of Co *K*-XAS, the theory does not reproduce the energy position of the highest fine structure above 5530 eV.

The Ca *K*-x-ray-absorption spectrum possesses a two-peak fine structure at around 4049 eV and several small peaks between 4060 eV and 4120 eV (Fig. 8). The theory reproduces well the energy position of this two-peak structure, however, with inverse intensities of the peaks. Our calculations give the larger intensity for the high-energy peak but the experiment shows the larger intensity for the low energy peak. The structure of Ca *K*-XAS reflects the energy distribution of the corresponding Ca 4*p* partial DOS (see the lower panel of Fig. 5). The partial DOS has two peaks at 12 eV and 15 eV above the Fermi level, which produce the major two-peak structure in Ca *K*-XAS.

We investigate also the effect of the electric quadrupole E_2 transi-

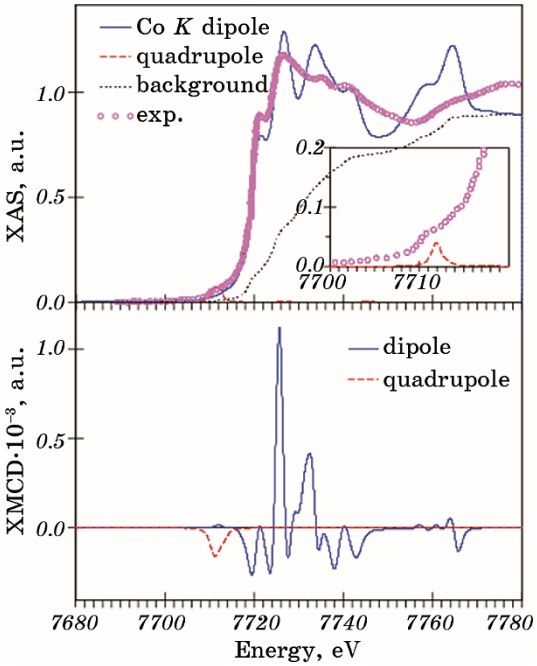

Fig. 6. Top panel: the experimental x-ray absorption spectrum (open circles) at the Co K-edge in $CaCo_3V_4O_{12}$ measured at 70 K [17] in comparison with the theoretically calculated one. The dotted black curve shows the background spectrum. Lower panel: the theoretically calculated XMCD of $CaCo_3V_4O_{12}$ at the Co K-edge. The dashed red curves show the quadrupole contributions to the spectra.

tions and magnetic dipole M_1 transitions on the XA and XMCD spectra at the transition metal K-edges. We found that the M_1 transitions are extremely small in comparison with the E_2 transitions and can be neglected. The E_2 transitions indeed contribute to the low energy XA spectra. Such transitions are responsible for the pre-peak structures of all three K-XA spectra shown in the inserts of Figs. 6, 7 and 8. The smallest E_2 contribution is found for the Co K-XA spectrum and the largest one for V K-XAS. The pre-peak in the Ca K-XA spectrum has a two-peak structure with the lower energy peak due to the dipole E_1 transitions and the higher energy one due to the quadrupole E_2 transitions (see the insert of Fig. 8).

The lower panels of Figures 6, 7 and 8 show the XMCD spectra at the Co, V, and Ca K-edges, respectively. The exchange splitting of the initial 1s core state is extremely small [35]; therefore, only the exchange and spin-orbit splitting of the final 2p states is responsible for the observed dichroism at the transition metal K-edge. For this reason, the dichroism is found to be very small, at least three orders of magnitude smaller than the XAS. The Co, V, and Ca K-XMCD spectra possess

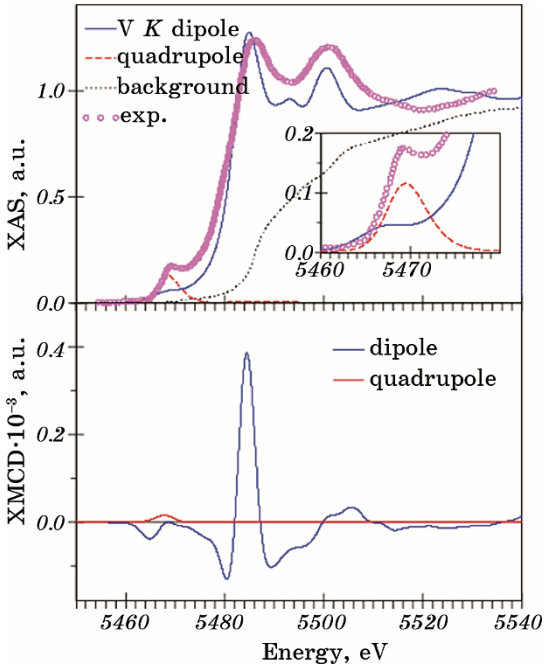

Fig. 7. Top panel: the experimental x-ray absorption spectrum (open circles) at the V K-edge in $CaCo_3V_4O_{12}$ measured at 70 K [17] in comparison with the theoretically calculated one. The dotted black curve shows the background spectrum. Lower panel: the theoretically calculated XMCD of $CaCo_3V_4O_{12}$ at the V K-edge. The dashed red curves show the quadrupole contributions to the spectra.

quite complicated structures with several minima and maxima. The largest contributions are found to come from the energy regions of the corresponding $3d$ states. The contributions of the quadrupole E_2 transitions to the XMCD spectra are one order of magnitude smaller than the dipole E_1 transitions and, hence, four orders of magnitude smaller than the intensity of the corresponding K-XAS. Therefore, the detection of the quadrupole transitions in the XMCD spectra of these $3d$ K-spectra is very close to impossible.

4. CONCLUSION

The electronic and magnetic structures as well as the XAS and x-ray magnetic circular dichroism of the A-site ordered perovskite $CaCo_3V_4O_{12}$ have been investigated theoretically within the DFT–GGA + U approach in the framework of the fully relativistic spin-polarized Dirac LMTO band-structure method.

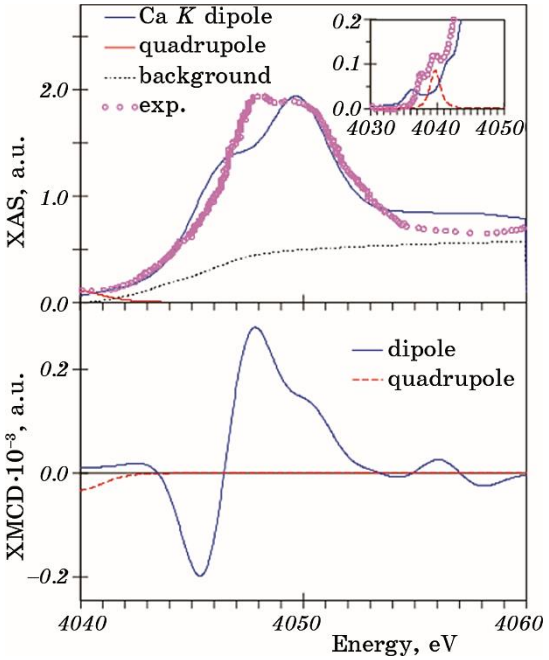

Fig. 8. Top panel: the experimental x-ray absorption spectrum (open circles) at the Ca K-edge in $CaCo_3V_4O_{12}$ measured at 70 K [17] in comparison with the theoretically calculated one. The dotted black curve shows the background spectrum. Lower panel: the theoretically calculated XMCD of $CaCo_3V_4O_{12}$ at the Ca K-edge. The dashed red curves show the quadrupole contributions to the spectra.

According to magnetic susceptibility and electrical resistivity measurements $CaCo_3V_4O_{12}$ possesses the AFM ordering and semiconducting behaviour at low temperature [19]. The collinear AFM $CaCo_3V_4O_{12}$ ground state calculated within the GGA and GGA + SOC approaches is metallic in contradiction to the experiment. Adding an on-site Coulomb repulsion on each of the Co and V ions results in a Mott-isolator-type electronic structure of $CaCo_3V_4O_{12}$. The energy band gap is rather small and equal to 0.109 eV at the Γ symmetry point. Both the Co^{2+} and V^{4+} ions are magnetic in Mott insulating $CaCo_3V_4O_{12}$. There is a substantial orbital moment over $1\mu_B$ at the Co site. Such a big orbital magnetic moment is due to a specific crystal structure of this double perovskite. The Co ion possesses the D_{2h} local symmetry in the rectangular CoO_4 plaquettes that leads to strong local anisotropy. Our calculations reveal that the Mott insulating character of the open-shell Co ions arises mostly through the d_{3z^2-1} orbital with a small amount of $d_{x^2-y^2}$. The 3d partial DOS of V ions is relatively small at the Fermi level.

We have studied the XAS and XMCD at the Co, V, and Ca K-edges.

The calculations show good agreement with the experimental measurements of the x-ray absorption spectra.

We have investigated the effect of the electric quadrupole E_2 and magnetic dipole M_1 transitions on the XA and XMCD spectra at the transition metal K-edges. We have found that the M_1 transitions are extremely small in comparison with the E_2 transitions and can be neglected. The E_2 transitions indeed contribute to the low energy part of XAS. Such transitions are responsible for the pre-peak structures of all three XA K-spectra. The smallest quadrupole contribution has been found for the Co K-XA spectrum and the largest for V K-XAS. The exchange splitting of the initial $1s$ core state is extremely small, therefore only the exchange and spin–orbit splitting of the final $2p$ states is responsible for the observed dichroism at the transition metal K-edge. For this reason, the dichroism has been found to be very small, at least three orders of magnitude smaller than the XA spectra. We have found that the largest quadrupole contributions come from the energy regions of the corresponding $3d$ states.

V. M. Antonov gratefully acknowledges the Max-Planck-Institut für Festkörperforschung in Stuttgart for the hospitality during his stay there.

REFERENCES

1. G. H. Jonker and J. H. van Santen, *Physica*, **16**, Iss. 3: 337 (1950).
2. E. O. Wollan and W. C. Koehler, *Phys. Rev.*, **100**: 545 (1955).
3. J. B. Goodenough, *Phys. Rev.*, **100**, 564 (1955).
4. M. Mochizuki and M. Imada, *New J. Phys.*, **6**: 154 (2004).
5. M. Imada, A. Fujimori, and Y. Tokura, *Rev. Mod. Phys.*, **70**: 1039 (1998).
6. A. M. Glazer, *Acta Cryst. B*, **28**: 3384 (1972).
7. C. J. Howard and H. T. Stokes, *Acta Cryst. B*, **54**: 782 (1998).
8. H. W. Eng, P. W. Barnes, B. M. Auer, and P. M. Woodward, *J. Solid State Chem.*, **175**: 94 (2003).
9. Beom Hyun Kim and B. I. Min, *Phys. Rev. B*, **80**: 064416 (2009).
10. A. Deschanvres, B. Raveau, and F. Tollemer, *Bull. Soc. Chim. Fr.*, **11**: 4077 (1967) (in French).
11. M. Marezio, P. D. Dernier, J. Chenavas, and J. C. Joubert, *J. Solid State Chem.*, **6**: 16 (1973).
12. C. C. Homes, T. Vogt, S. M. Shapiro, S. Wakimoto, and A. P. Ramirez, *Science*, **293**: 673 (2001).
13. Y. W. Long, N. Hayashi, T. Saito, M. Azuma, S. Muranaka, and Y. Shimakawa, *Nature*, **458**: 60 (2009).
14. R. D. Johnson, L. C. Chapon, D. D. Khalyavin, P. Manuel, P. G. Radaelli, and C. Martin, *Phys. Rev. Lett.*, **108**: 067201 (2012).
15. Y Shimakawa, *Inorg. Chem.*, **47**: 8562 (2008).
16. H. Shiraki, T. Saito, M. Azuma, and Y. Shimakawa, *J. Phys. Soc. Jpn.*, **77**: 064705 (2008).

17. S. V. Ovsyannikov, E. Bykova, A. Pakhomova, D. P. Kozlenko, M. Bykov, S. E. Kichanov, N. V. Morozova, I. V. Korobeinikov, F. Wilhelm, A. Rogalev, A. A. Tsirlin, A. V. Kurnosov, Y. G. Zainulin, N. I. Kadyrova, A. P. Tyutyunnik, and L. Dubrovinsky, *Inorg. Chem.*, **56**: 6251 (2017).
18. C. T. G. Petit, R. Lan, P. I. Cowin, J. T. S. Irvine, and S. Tao, *J. Mater. Chem.*, **21**: 525 (2011).
19. S. V. Ovsyannikov, Y. G. Zainulin, N. I. Kadyrova, A. P. Tyutyunnik, A. S. Semenova, D. Kasinathan, A. A. Tsirlin, N. Miyajima, and A. E. Karkin, *Inorg. Chem.*, **52**: 11703 (2013).
20. V. I. Anisimov, J. Zaanen, and O. K. Andersen, *Phys. Rev. B*, **44**: 943 (1991).
21. G. Y. Guo, H. Ebert, W. M. Temmerman, and P. J. Durham, *Phys. Rev. B*, **50**: 3861 (1994).
22. V. Antonov, B. Harmon, and A. Yaresko, *Electronic Structure and Magneto-Optical Properties of Solids* (Dordrecht: Springer: 2004).
23. E. Arola, M. Horne, P. Strange, H. Winter, Z. Szotek, and W. M. Temmerman, *Phys. Rev. B*, **70**: 235127 (2004).
24. H. B. Rhee and W. E. Pickett, *Phys. Rev. B*, **90**: 205119 (2014).
25. I. Leonov, A. N. Yaresko, V. N. Antonov, U. Schwingenschlögl, V. Eyert, and V. I. Anisimov, *J. Phys.: Condens. Matter*, **18**: 10955 (2006).
26. V. N. Antonov, B. N. Harmon, A. N. Yaresko, and A. P. Shpak, *Phys. Rev. B*, **75**: 184422 (2007).
27. V. N. Antonov, A. N. Yaresko, and O. Jepsen, *Phys. Rev. B*, **81**: 075209 (2010).
28. B. J. Ruck, H. J. Trodahl, J. H. Richter, J. C. Cezar, F. Wilhelm, A. Rogalev, V. N. Antonov, Binh Do Le, and C. Meyer, *Phys. Rev. B*, **83**: 174404 (2011).
29. O. Krogh Andersen, *Phys. Rev. B*, **12**: 3060 (1975).
30. V. V. Nemoshkalenko, A. E. Krasovskii, V. N. Antonov, Vl. N. Antonov, U. Fleck, H. Wonn, and P. Ziesche, *Phys. status solidi (b)*, **120**: 283 (1983).
31. J. P. Perdew, K. Burke, and M. Ernzerhof, *Phys. Rev. Lett.*, **77**: 3865 (1996).
32. P. E. Blöchl, O. Jepsen, and O. K. Andersen, *Phys. Rev. B*, **49**: 16223 (1994).
33. A. N. Yaresko, V. N. Antonov, and P. Fulde, *Phys. Rev. B*, **67**: 155103 (2003).
34. J. L. Campbell and Tibor Papp, *At. Data Nucl. Data Tables*, **77**: 1 (2001).
35. H. Ebert, *J. Phys.: Condens. Matter*, **1**: 9111 (1989).